Post-decision processing in primate prefrontal cortex influences subsequent choices on an auditory decision-making task

Joji Tsunada[1], Yale E. Cohen[1,2,3*], and Joshua I. Gold[2*]

[1]Departments of Otorhinolaryngology, [2]Neuroscience, and [3]Bioengineering, University of Pennsylvania, Philadelphia, PA 19104

*both authors contributed equally

Abstract

Perceptual decisions do not occur in isolation but instead reflect ongoing evaluation and adjustment processes that can affect future decisions. However, the neuronal substrates of these across-decision processes are not well understood, particularly for auditory decisions. We measured and manipulated the activity of choice-selective neurons in the ventrolateral prefrontal cortex (vlPFC) while monkeys made decisions about the frequency content of noisy auditory stimuli. As the decision was being formed, vlPFC activity was not modulated strongly by the task. However, after decision commitment, vlPFC population activity encoded the sensory evidence, choice, and outcome of the current trial and predicted subject-specific choice biases on the subsequent trial. Consistent with these patterns of neuronal activity, electrical microstimulation in vlPFC tended to affect the subsequent, but not current, decision. Thus, distributed post-commitment representations of graded decision-related information in prefrontal cortex can play a causal role in evaluating past decisions and biasing subsequent ones.

Perceptual decision-making is a deliberative process that produces a categorical judgment regarding the presence, identity, and other features of a sensory stimulus[1]. This deliberation often requires resolving potentially ambiguous interpretations of the current sensory stimulus with expectations that can be learned by evaluating prior decisions and their outcomes[2, 3]. This learning process can result in sequential effects on a subject's choices and response times (RTs) when they participate in psychophysical tasks that require one decision after another[4-12]. Because sequential effects can be present even when a task is designed to generate independent trial-by-trial choices and after extensive training, these effects may represent fundamental, ongoing processes that evaluate and adjust decisions to account for changes in the sensory environment, reward contingencies, and other factors[3, 13]. Although neuronal substrates of these sequential effects have been identified in several brain regions[2, 4-8, 14-19], the exact nature of the signals that the brain uses to support these effects is still not well understood.

In a previous study, we demonstrated that neurons in middle-lateral (ML) and anterolateral (AL) belt regions of the auditory cortex encode key features of the sensory evidence needed to solve an auditory-decision task[20]. This task required monkeys to report whether a tone-burst sequence contained more low- or high- frequency tone bursts. We found that both AL and ML neurons were modulated by the frequency content of the tone-burst sequence. However, in AL, but not ML, neuronal activity was weakly related to choice, and microstimulation biased the monkeys' choices. These findings suggest a more direct role for AL in the decision process than for ML. They are also consistent with the idea that AL provides evidence for the decision but leave open the question of where and how in the brain is this evidence interpreted and combined with other information to form the decision[1].

The goal of the present study was to identify a role for the ventrolateral prefrontal cortex (vlPFC) in forming this auditory decision. We targeted vlPFC because it receives direct and

indirect projections from AL and is situated at the apex of the ventral auditory pathway, which is commonly thought to mediate auditory perception and decision-making[20-25]. Here, we show that, contrary to our initial expectations, vlPFC neurons do not appear to encode information relevant to forming the current decision. Instead, vlPFC population activity can encode rich, graded information about the just-completed decision process, including the strength of the sensory evidence, the resulting choice, and whether or not it was correct. These signals, which were apparent from just after the decision was formed until after feedback was received, were closely and causally related to the subsequent decision in a manner that matched each monkey's idiosyncratic choice strategy. Together, these results imply a role for the vlPFC in the ongoing evaluation and adjustment of auditory decisions.

Results

We recorded and manipulated vlPFC spiking activity in two monkeys while they reported whether a noisy auditory stimulus contained more low- or high-frequency tone bursts (Fig. 1a,b). A primary benefit of this task is that we could control the strength of the sensory evidence (the fraction of low or high tone bursts in a given stimulus; i.e., coherence) and relate that evidence to the monkeys' choices and to vlPFC activity. These monkeys participated in our previous study[20], but the behavioral and neuronal data presented here have not been reported previously.

Idiosyncratic choice-bias behavior

Both monkeys' choice accuracy and RTs depended systematically on stimulus coherence (monkey T: *n*=29 behavioral sessions; monkey A: *n*=39 behavioral sessions; Fig. 2a,b). For high-coherence stimuli, both monkeys almost always reported the correct answer with relatively short RTs. As absolute coherence decreased, performance accuracy decreased and RT increased. These psychometric (choice) and chronometric (RT) data were well described jointly by a drift-diffusion model (DDM; Fig. 2a,b, pink lines)[1, 26]. The DDM describes the process of forming a decision by accumulating incoming auditory (sensory) evidence over time to one of two pre-defined boundaries and accounts for both the choice (which boundary was reached) and the decision time (when the boundary was reached). These fits provided a consistently good match to the data (average deviance was 11.82 for monkey T [χ^2-cumulative distribution, $p< 0.001$] and 10.99 for monkey A [$p<0.001$])[27]. Moreover, because these fits partitioned the monkeys' RTs into decision and non-decision times (Fig. 2a,b), it facilitated our ability to identify the contributions of vlPFC activity to decision-making[28]. In general, for both choices, decision times increased as the absolute stimulus coherence decreased, whereas non-decision times

tended to be strongly asymmetric for the two choices, reflecting the different joystick movements. In subsequent analyses, we define the time of the "decision commitment" as the end of the decision time plus an additional 50 ms to account for stimulus encoding[20].

We also identified idiosyncratic sequential choice biases for the two monkeys. Monkey T tended to use a "win-stay, lose-switch" strategy (top panels in Fig. 2c, d). That is, this monkey had a tendency to repeat the previous choice if that choice was correct and rewarded but switch choices if the previous choice was an error and not rewarded. This tendency was seen in both the pooled data (Fig. 2c; logistic regression: β_0 [bias]=-0.46, p<0.01; β_1 [stimulus coherence]=2.50, p<0.01; β_2 [previous trial was correct]=0.14, p<0.01; β_3 [previous trial was incorrect]=-0.30, p<0.01) and in the session-by-session data (Fig. 2d; median β_0=-0.5, Wilcoxon sign-rank test, p=0.04; β_1=3.73, p<0.01; β_2=0.27, p<0.01; β_3=-0.39, p=0.03).

In contrast, monkey A tended to use a "win-switch" strategy (bottom panels in Fig. 2c, d). That is, this monkey had a tendency to switch choices following a correct choice. Once again, this result was evident in both the pooled data (Fig. 2c, β_0=-0.45, p<0.01; β_1=3.16, p<0.01; β_2=-0.19, p<0.01; β_3=-0.02, p=0.88) and in the session-by-session data (Fig. 2d, β_0=0.5, p<0.01; β_1=3.63, p<0.01; β_2=-0.2, p<0.01; β_3=-0.17, p=0.63). For both monkeys, we could not identify similar systematic effects on sequential RTs.

Post-decision neuronal representations of choice, outcome, and stimulus strength

Identifying the neuronal substrates of a perceptual decision typically involves identifying at least three forms of selectivity: (1) selectivity for choice, reflecting the consequence of the decision process; (2) selectivity for whether the choice was correct or an error, reflecting a closer association with perception than just sensory or motor processing; and (3) selectivity for stimulus strength, because the process of forming the decision should reflect not just the

categorical choice but also the strength of the evidence used to arrive at that choice[1]. As detailed below, we identified all three forms of selectivity in vlPFC activity but only after the time of decision commitment on the current trial.

Individual vlPFC neurons had task-driven activity that was modulated selectively by the monkeys' low- versus high-frequency choices (single-unit examples are shown in Fig. 3 and summary population data are shown in Fig. 4). Across the population of recorded neurons, the onset of choice selectivity for individual neurons (which were recorded in separate sessions and across the two monkeys) spanned the time from the inferred decision commitment through the motor response (joystick movement) and to the time of reward delivery on correct trials. This selectivity included preferences for both high- and low-frequency choices. We identified 13 and 15 high-frequency (ipsilateral)-preferring neurons in monkeys T and A, respectively; and 10 and 14 low-frequency (contralateral)-preferring neurons, respectively (there was not any evidence for laterality: χ^2-test for H_0: no difference in the proportion of contralateral- and ipsilateral preferring neurons, $p>0.05$ for both monkeys).

The choice selectivity of individual neurons was also affected by the outcome of the current trial. Specifically, choice selectivity tended to be higher on correct trials than on error trials (Fig. 5). This difference in choice selectivity could not be explained trivially by neuronal modulations resulting from the presence or absence of the juice reward, because this difference was apparent even before reward delivery. Instead, this difference likely reflected differences in decision processing on correct versus error trials, including more uncertainty in the neuronal representation of the sensory evidence.

In contrast to these single-neuron modulations by choice and outcome, the responses of individual vlPFC neurons were not selective for stimulus coherence. In particular, we found that, at any given time point, at most 6 vlPFC neurons were modulated by stimulus coherence for either preferred or non-preferred choices (Fig. 4b). However, we found a more robust

representation of stimulus coherence at the level of population neuronal activity (Fig. 6). The intuition for this discrepancy can be seen in Fig. 4a: the fraction of neurons with choice selectivity was systematically smaller with decreasing coherence, implying that population-level signals were dependent on coherence. Although these effects did not correspond to statistically reliable differences in single-neuron coherence selectivity, there was enough information across the population of neurons for a linear classifier to decode both stimulus coherence and choice at well above chance levels following decision commitment (Fig. 6).

Thus, the vlPFC population had access to the key features of the decision process, including the strength of the evidence used to form the decision, the choice, and whether the choice was correct or an error. These signals were not apparent before the decision commitment, implying that they did not contribute to the formation of the current decision. Instead, the timing of these signals suggests that they may play a role in post-decision processing that can link one decision to the next decision.

Post-decision vlPFC activity encodes subsequent choice biases

Single-unit activity in the post-decision epoch was selective for the current choice but also for the subsequent choice. Moreover, this selectivity matched each monkey's idiosyncratic choice biases (Fig. 2c,d), particularly following correct trials. Monkey T's tendency to repeat rewarded trials was reflected in post-decision neuronal responses that tended to be slightly larger on trials in which the subsequent choice matched the neuron's choice selectivity (Fig. 7a). For example, if a neuron tended to respond more for a high-frequency choice in the post-decision epoch of the current trial, its response tended to be slightly higher when the monkey made a high-frequency choice on the subsequent trial. In contrast, monkey A's tendency to switch after rewarded trials was reflected in neuronal responses that tended to be slightly

smaller on trials in which the subsequent choice matched the neuron's choice selectivity (Fig. 7b). These effects had slightly different time courses in the two monkeys. Nonetheless, in both cases, these effects occurred after the decision commitment on correct trials, thus corresponding to a time period when evaluative processing could be used to adjust subsequent decisions. We could not identify similarly reliable effects following error trials, possibly reflecting the much smaller data sets from those trials.

Electrical microstimulation biased subsequent choice

We used electrical microstimulation to test whether vlPFC activity plays a causal role in driving choice biases on the subsequent trial. We applied microstimulation from the time of stimulus onset until just after the behavioral response on a randomly selected 50% of trials in a subset of sessions (n=11 sessions for monkey T, 21 sessions for monkey A). Despite the fact that this protocol was designed to test our initial hypothesis that vlPFC activity encoded formation of the current decision (and thus microstimulation was applied primarily during decision formation), we found that microstimulation did not systematically affect either the choice bias or the sensitivity of the decision on the current trial (single-site examples are shown in Fig. 8a,b; population summaries are shown in Fig. 8c,d).

Instead, we found that microstimulation induced choice biases on the subsequent decision that depended systematically on the choice selectivity of the recorded vlPFC neuron at the microstimulation site. If microstimulation was applied at a site that was tuned for low-frequency choices, it tended to cause a low-choice bias on the subsequent trial (single-site example in Fig. 8e). In contrast, if microstimulation was applied at a site that was tuned for high-frequency choices, it tended to cause a high-choice bias on the subsequent trial (single-site example in Fig. 8f). Accordingly, across the population of microstimulation sites from both

monkeys, the induced choice bias on the subsequent trial was correlated positively with the strength and direction of choice selectivity at the given site (Fig. 8g), without any concomitant, systematic change in psychometric sensitivity (Fig. 8h).

These microstimulation effects also depended on more specific choice patterns that differed for the two monkeys. When microstimulation was applied on a trial that resulted in a correct high choice, the subsequent choice tended to be biased in the same direction as the choice selectivity of the neuron recorded at the site of microstimulation for both monkeys (monkey T: Spearman's rank correlation coefficient $\rho=0.90$, $p<0.001$; monkey A: $\rho=0.61$, $p=0.04$). When microstimulation was applied on a trial that resulted in a correct low choice, a similar effect was found only for one of the two monkeys (monkey T: $\rho=0.91$, $p<0.001$; monkey A: $\rho=0.1$, $p=0.75$). Together, these effects are consistent with the hypothesis that vlPFC activity is causally involved in evaluative processing that adjusts subsequent decisions.

Discussion

We combined behavioral modeling, neuronal recordings, and electrical microstimulation to identify causal contributions of the primate vlPFC to a simple perceptual decision about the frequency content of a sequence of tone bursts. vlPFC activity had many of the hallmarks of a decision variable, including modulations by choice, outcome (i.e., whether the choice was correct or incorrect), and the strength of the sensory evidence used to arrive at the choice. However, these forms of selectivity were not evident until after the time of the decision commitment and thus were inconsistent with a role in forming the current decision. Instead, this activity was modulated by the monkeys' subsequent choices in a manner that reflected their idiosyncratic choice biases. Further, there was a systematic relationship between vlPFC choice selectivity and the effects of microstimulation on the monkeys' choices on the subsequent, but not current, trial. Together, these results imply that post-decision vlPFC activity can play a role in evaluating the prior judgment, generating subject-specific internal biases, and updating subsequent decision-making strategies.

The post-decision signals that we identified appear to be a form of "decision-trace" activity that has been identified in a number of cortical and subcortical areas, including parts of the prefrontal cortex[7, 8, 14-16, 29-31]. These signals represent information about the immediately preceding decision, which in some cases is used as part of feedback-driven learning process that adjusts future decisions based on a comparison between the expected and actual outcome[32]. In our study, we found a strong, population-level representation of information related to the preceding decision that could, in principle, be used to compute a confidence or prediction signal. This representation was also modulated by trial outcome, but this modulation was apparent even before feedback was given. Thus, this outcome modulation seems more likely to represent uncertainty in the information used to form the decision than a direct comparison to feedback, which may occur elsewhere in the brain for this task[15, 16, 33, 34].

Nevertheless, we found reliable and causal relationships between these post-decision signals and choice behavior on the subsequent trial, a finding that is reminiscent of recent studies showing that parts of the posterior parietal cortex in rodents also drive history-dependent choice biases on an auditory-discrimination task[8]. Our results extend those findings to establish a role for the primate vlPFC in subject-specific versions of these kinds of history-dependent choice biases.

Our findings of primarily post-decision processing in the vlPFC are somewhat inconsistent with other studies that have implicated the PFC in forming auditory and other decisions[24, 35-38]. The reasons for this discrepancy are not clear. One possible reason is that we sampled a different PFC population than in other studies. Another possibility is that previous reports of decision-related activity were also largely post-decisional. However, accounting for this possibility is not straightforward: because previous studies did not use RT tasks, it is difficult to interpret those results in terms of whether the reported decision-related signals occurred before or after the decision was formed on each trial[24, 35, 39].

We still do not know the brain regions that form the decision for our task and consequently do not understand the mechanisms underlying these decisions. Because the monkeys' choice and RT patterns reflected both the temporal accumulation of sensory evidence and sequential choice biases, we would expect these putative brain regions to implement two key operations. First, they should temporally accumulate the sensory evidence that is represented in the auditory cortex, particularly AL[20]. Second, they should combine this accumulated evidence with historical sensory, outcome, and choice information such as is represented in vlPFC to drive sequential choice biases[7, 8, 15, 16, 38].

Future studies that focus on identifying neuronal activity related to decision formation will likely benefit not only from an RT design to better identify the temporal epoch of decision formation but also a more thorough understanding of the dynamic and possibly idiosyncratic

nature of the computations used to convert incoming sensory evidence into the categorical choice[13, 28]. These studies might also benefit from analyses that focus on substrates of subject-specific decision strategies, which help to establish the behavioral relevance of the neuronal signals[9, 11, 13]. For example, in the present study, we found that our monkeys had different strategies of sequential choice biases (win-stay for monkey T versus win-switch for monkey A; Fig. 2). These subject-specific choice biases have been reported previously in humans and animals, but their neuronal correlates have yet to be fully explained[9, 11, 15]. Because the monkeys' idiosyncratic behavioral strategies corresponded to different patterns of choice selectivity in vlPFC, it implies that these signals may play a behaviorally relevant, subject-specific role in the evaluation and adjustment of the decision process, rather than providing a simple memory trace of common components of the decision process[31, 40].

Finally, it is worth emphasizing that in our study, the representations in the vlPFC of critical decision-related variables (i.e., choice, outcome, and the strength of the sensory evidence) were not all evident in the spiking activity of individual neurons but instead at the populations level. The time course of these representations was also distributed across the neuronal population: different neurons (in our case, recorded in separate sessions) responded selectively at relatively restricted times with onsets that tiled the task epoch in a manner similar to other reports of working memory in the prefrontal cortex[41-45]. These population-level representations highlight the importance of conducting population recordings and analyses to identify and understand complex decision-related computations in the brain[46-51].

Methods

The University of Pennsylvania Institutional Animal Care and Use Committee approved all of the experimental protocols. All surgical procedures were conducted using aseptic surgical techniques and with the monkeys kept under general anesthesia. A supplementary methods checklist is available. The authors were not blind to group allocation during the experiment and when assessing the data outcomes.

Two male monkeys (*Macaca mulatta*; monkey T [15 years old] and monkey A [14 years old]) participated in this study. Both were used in a previous study of auditory cortex[20], and monkey T was also used in a previous study of vlPFC[52]. In each session, the monkey was seated in a primate chair. A calibrated speaker (model MSP7, Yamaha) was placed in front of the monkey at eye level. The monkey moved a joystick, which was attached to the primate chair, to indicate their behavioral report. All experimental sessions took place in an RF-shielded room that had sound-attenuating walls and echo-absorbing foam on the inner walls.

IDENTIFICATION OF VENTROLATERAL PREFRONTAL CORTEX. Prior to implantation of a recording chamber, the stereotactic location of vlPFC, which includes Brodmann area 45 and 46 (Fig. 1b), was identified through structural MRI scans[53]. We centered the recording chamber over this cortical location. vlPFC was further identified by its auditory responses[54, 55].

AUDITORY TASKS AND STIMULI. Auditory stimuli were generated using Matlab (The Mathworks Inc.) and the RX6 digital-signal-processing platform (TDT Inc.).

Frequency tuning. We measured the frequency tuning of vlPFC recording sites by presenting individual tone bursts in a random order while the monkey listened passively. The tone bursts (100-ms duration with a 5-ms $\cos^2$ ramp; 65 dB SPL) varied between 0.3–12 kHz in one-third octave steps. The monkeys did not receive any rewards during this time period.

Low-high task. The low-high task was a single-interval, two-alternative forced-choice discrimination task that required a monkey to report whether a temporal sequence of tone bursts contained more low-frequency or high-frequency tone bursts (Fig. 1a). A trial began with the monkey grasping the joystick. After a 400-ms delay, we presented a sequence of tone bursts (50-ms duration; 5-ms $\cos^2$ ramp; 10-ms inter-burst interval). The monkey moved the joystick: (1) to the right to report that the sequence contained more low-frequency tone bursts or (2) to the left to report that the sequence contained more high-frequency tone bursts. The monkey could report its choice at any time after stimulus onset.

On a trial-by-trial basis, we randomly varied the proportion of low- and high-frequency tone bursts (coherence) in the auditory stimulus. We varied coherence from -100% (all low-frequency tone bursts) to +100% (all high-frequency tone bursts), with 0% coherence corresponding to 50% of the tone bursts randomly assigned as low or high frequency. Based on each trial's coherence, a tone-burst sequence was generated by randomly assigning the frequency of each tone burst to the low- or high-frequency value.

All correct choices were rewarded with a drop of juice. For trials with fully ambiguous stimuli (50% coherence), the monkey was rewarded on 50% of randomly selected trials, independent of their behavioral report. The monkey's reward did not depend on the speed of the behavioral report, only its accuracy. Errors resulted in an increased (by 2 s) inter-trial interval.

RECORDING METHODOLOGY. At the start of each recording session, a tungsten microelectrode (~1.0 MΩ @ 1 kHz; FHC Inc.) or a tetrode (0.5-0.8 MΩ @ 1 kHz; Thomas RECORDING GmbH) was placed in a skull-mounted microdrive (Narishige, MO-95) and then lowered into the brain through a recording chamber. All neuronal signals were sampled at 24 kHz, band-pass filtered between 0.7–7.0 kHz (RA16PA and RZ2, TDT Inc.), and stored for online and offline analyses. OpenEx (TDT Inc.), Labview (NI Inc.), and Matlab (The Mathworks) software synchronized behavioral control with stimulus production and data collection. Single-

neuron activity was isolated from the neuronal signals with on-line (OpenSorter, TDT Inc.) and off-line (Offline Sorter, Plexon Inc.) spike-sorting programs.

DATA-COLLECTION STRATEGY. In our initial sessions, once multi-unit spiking activity was detected, we presented tone bursts to generate a frequency-tuning curve. However, because most vlPFC neurons were not frequency tuned (only 3 out of 65 tested sites, Kruskal-Wallis test, $p<0.05$), we generally used one of three standardized sets of low and high frequencies: (1) 1000 and 3000 Hz (n=52 sessions); (2) 1250 and 2500 Hz (n=40); and (3) an arbitrary value <1750 Hz and a value 1–3 octaves above the selected low frequency (n=11). Next, the monkey participated in the low-high task. We varied stimulus coherence randomly on a trial-by-trial basis.

During sessions with electrical microstimulation, we delivered negative-leading bipolar current pulses (rate: 300 Hz; pulse duration: 250 µs; amplitude: 25-75 µA) on 50% of randomly interleaved trials using a dual-output square-pulse stimulator (Grass S88) and two optical isolation units (Grass PSIU6)[56, 59]. Microstimulation started with stimulus onset and terminated at joystick movement. Because microstimulation trials were rewarded using the same schedule as non-microstimulation trials, the monkeys were not incentivized to respond differently during microstimulation trials than during non-microstimulation trials.

BEHAVIORAL ANALYSES. For all analyses, stimulus coherence was calculated from the actual proportion of low- and high-frequency tone bursts that were presented from stimulus onset until the monkey indicated its choice by moving the joystick on a given trial.

Drift-diffusion model. Psychophysical and chronometric data were fit to a standard drift-diffusion model (DDM), which models a decision process in which noisy evidence is accumulated over time until it reaches a fixed bound[56, 60-66]. This version of the model had five free parameters: k, A, B, F_1, and F_2. k governed the stimulus sensitivity of the moment-by-

moment sensory evidence. The evidence had a Gaussian distribution $N(\mu,1)$ in which the mean μ scaled with the stimulus coherence (COH): $\mu = k \times COH$. The decision variable was the temporal accumulation of this momentary sensory evidence. A decision occurred when this decision variable reached a decision bound ($+A$ or $-B$, which corresponded to a high- and low-frequency choice, respectively). "Decision time" was the time between stimulus onset and the crossing of either bound. Response time (RT; which was the time from stimulus onset to the onset of joystick movement) could also be defined as the sum of this decision time and a "non-decision time" (F_1 for a high-frequency choice and F_2 for a low-frequency choice). Non-decision time includes processes such as stimulus encoding and motor preparation. We defined the time of "decision commitment" as the end of the decision time plus an additional 50 ms to account for sensory latency[20]. The probability that the decision variable crossed the $+A$ bound first is $\frac{e^{2\mu B}-1}{e^{2\mu B}-e^{-2\mu A}}$. The average decision time is $\frac{A+B}{\mu} \times \coth\big(\mu(A+B)\big) - \frac{B}{\mu}\coth(\mu B)$ for high-frequency choices and $\frac{A+B}{\mu} \times \coth\big(\mu(A+B)\big) - \frac{A}{\mu}\coth(\mu A)$ for low-frequency choices.

Logistic analysis of psychophysical data. We also used a logistic function to fit psychophysical choice data[56, 67, 68]. This function related the probability (p) that the monkey reported high-frequency choices as a function of coherence (COH): $p = L + (1 - 2L)\frac{1}{1+e^{-(\beta_{COH} * COH + \beta_0)}}$. L represents the upper and lower asymptotes (lapse rates) of the logistic function. β_{COH} quantifies the effect of coherence on the monkey's choices and governs the slope of the psychometric function. β_0 quantifies choice biases and governs the function's horizontal position. In a separate analysis, we used indicator variables to determine additional choice biases conditioned on the outcome of the previous trial: (1) if the choice on the previous trial was correct (correct high choice = +1, correct low choice = -1, error = 0), and (2) if the choice on the previous trial was incorrect (error high choice = +1, error low choice = -1, correct = 0). If a monkey repeated the same choice, the coefficient values of the indicator variables would be

positive. If a monkey switched one's choice, the coefficients values would be negative. For our session-by-session analyses (Fig. 2d), we removed some sessions from this analysis due to the small number of trials per condition. A maximum-likelihood procedure fit the logistic function to the behavioral data.

To quantify the effects of microstimulation on behavior, we fit the logistic function (with additional indicator variables and assumed that each session had a single lapse rate across all microstimulation and non-microstimulation trials) to choice data from subsets of trials in individual sessions and tested whether the choice bias and perceptual sensitivity differed: (1) when microstimulation was applied on the current trial (+1) versus when it was not applied (0) and (2) when microstimulation was applied on the previous trial (+1) versus when it was not applied (0). "Choice bias" was defined as the horizontal shift of psychometric functions. More specifically, the shift was calculated as the difference between stimulus coherences that elicited 50% high-frequency choices. "Perceptual sensitivity" was defined as the change in the slope of the psychometric function determined from the 25% and 75% high-frequency choice points.

NEURONAL ANALYSES. We did not use statistical methods to predetermine sample sizes. Our sample sizes were similar to those reported in previous publications, including our recent study of auditory cortex[20, 69, 70].

Single-neuron choice selectivity. To identify if and when each neuron had statistically significant choice-related activity, we performed a running Wilcoxon rank-sum test for each pair of stimulus coherence bins with the same magnitude but different signs (H_0: firing rates elicited by the coherence pair are the same, $p<0.05$, FDR corrected)[15, 16]. For correct trials, this convention equates the sign of stimulus coherence with the sign of the associated choice. That is, negative values map onto low-frequency stimuli and choices, whereas positive values map onto high-frequency stimuli and choices. We analyzed choice-related activity in 300-ms time bins, shifted in 10-ms steps. Choice selectivity was quantified using an ROC analysis, which

measures the ability of an ROC-based ideal observer to predict a monkey's choice based only on firing rates[20, 24, 71].

Linear-classifier analysis for population activity. We used linear classifiers[72, 73] to test whether vlPFC population activity was modulated by stimulus coherence (using four binned ranges of coherence: [1] -100% – -50%, [2] -50% – 0%, [3] 0% – +50%, and [4] +50% – +100%) or by behavioral choice (high- versus low-frequency choices across all coherences). This analysis was restricted to data generated on correct trials only to help to ensure that we could quantify the effects of stimulus coherence and behavioral choice on vlPFC population activity and not outcome effects (correct versus incorrect trials). For each classifier and for each neuron, we z-scored firing rate and randomly subsampled the trials so that we had equal number of trials for each condition. Each classification analysis underwent a 10-fold cross-validation procedure to avoid overfitting. This procedure divided the neuronal data into 10 groups in an iterative fashion, such that one group was a test set and the remaining nine formed a training set. We implemented a linear read-out procedure in which we fit the training set to a linear hyperplane that separated the population response vectors corresponding to the two choices. For the coherence classifier, we implemented a "one-versus-all" classification in which we built four classifiers (one for each binned coherence range) and trained each of them, in an iterative fashion, to discriminate between one particular coherence range versus all of the remaining three coherence ranges. Using the test data, we identified which of the four classifiers had the best performance and report average performance across coherence. For both classifiers, we calculated the fraction of times that the test data was classified correctly and report average performance over 1000 different instantiations of a classifier.

CODE AVAILABILITY. The data analyses were performed in Matlab; this code is available https://github.com/CohenAuditoryLab/Joji.

Acknowledgements

We thank Dr. Andrew Liu for helping of experimental setup, animal training, and neuronal recording. We also thank Dr. Long Ding for providing data analysis programs and for helpful discussions. YEC and JIG were supported by grants from the NIH.

Author contributions

JT, YEC, and JIG designed the study, analyzed the data, and wrote the paper. JT collected the experimental data.

References

1. Gold, J.I. & Shadlen, M.N. The neural basis of decision making. *Annu Rev Neurosci* **30**, 535-574 (2007).
2. Fecteau, J.H. & Munoz, D.P. Exploring the consequences of the previous trial. *Nat Rev Neurosci* **4**, 435-443 (2003).
3. Gold, J.I. & Stocker, A.A. Visual Decision-Making in an Uncertain and Dynamic World. *Annu Rev Vis Sci* **3**, 227-250 (2017).
4. Gold, J.I., Law, C.T., Connolly, P. & Bennur, S. The relative influences of priors and sensory evidence on an oculomotor decision variable during perceptual learning. *J Neurophysiol* **100**, 2653-2668 (2008).
5. Marcos, E.*, et al.* Neural variability in premotor cortex is modulated by trial history and predicts behavioral performance. *Neuron* **78**, 249-255 (2013).
6. Akaishi, R., Umeda, K., Nagase, A. & Sakai, K. Autonomous mechanism of internal choice estimate underlies decision inertia. *Neuron* **81**, 195-206 (2014).
7. Hwang, E.J., Dahlen, J.E., Mukundan, M. & Komiyama, T. History-based action selection bias in posterior parietal cortex. *Nat Commun* **8**, 1242 (2017).
8. Akrami, A., Kopec, C.D., Diamond, M.E. & Brody, C.D. Posterior parietal cortex represents sensory history and mediates its effects on behaviour. *Nature* **554**, 368-372 (2018).
9. Busse, L.*, et al.* The detection of visual contrast in the behaving mouse. *J Neurosci* **31**, 11351-11361 (2011).
10. Fischer, J. & Whitney, D. Serial dependence in visual perception. *Nat Neurosci* **17**, 738-743 (2014).
11. Abrahamyan, A., Silva, L.L., Dakin, S.C., Carandini, M. & Gardner, J.L. Adaptable history biases in human perceptual decisions. *Proc Natl Acad Sci U S A* **113**, E3548-3557 (2016).
12. Luu, L. & Stocker, A.A. Post-decision biases reveal a self-consistency principle in perceptual inference. *Elife* **7** (2018).
13. Fan, Y., Gold, J.I. & Ding, L. Ongoing, rational calibration of reward-driven perceptual biases. *Elife* **7** (2018).
14. Barraclough, D.J., Conroy, M.L. & Lee, D. Prefrontal cortex and decision making in a mixed-strategy game. *Nat Neurosci* **7**, 404-410 (2004).
15. Ding, L. & Gold, J.I. Caudate encodes multiple computations for perceptual decisions. *J Neurosci* **30**, 15747-15759 (2010).
16. Ding, L. & Gold, J.I. Neural Correlates of Perceptual Decision Making before, during, and after Decision Commitment in Monkey Frontal Eye Field. *Cereb Cortex* **22**, 1052-1067 (2011).
17. Carnevale, F., de Lafuente, V., Romo, R. & Parga, N. Internal signal correlates neural populations and biases perceptual decision reports. *Proc Natl Acad Sci U S A* **109**, 18938-18943 (2012).
18. St John-Saaltink, E., Kok, P., Lau, H.C. & de Lange, F.P. Serial Dependence in Perceptual Decisions Is Reflected in Activity Patterns in Primary Visual Cortex. *J Neurosci* **36**, 6186-6192 (2016).
19. Lueckmann, J.M., Macke, J.H. & Nienborg, H. Can Serial Dependencies in Choices and Neural Activity Explain Choice Probabilities? *J Neurosci* **38**, 3495-3506 (2018).
20. Tsunada, J., Liu, A.S., Gold, J.I. & Cohen, Y.E. Causal contribution of primate auditory cortex to auditory perceptual decision-making. *Nat Neurosci* **19**, 135-142 (2016).
21. Romanski, L.M.*, et al.* Dual streams of auditory afferents target multiple domains in the primate prefrontal cortex. *Nat Neurosci* **2**, 1131-1136 (1999).
22. Hackett, T.A., Stepniewska, I. & Kaas, J.H. Prefrontal connections of the parabelt auditory cortex in macaque monkeys. *Brain Res* **817**, 45-58. (1999).

23. Rauschecker, J.P. & Tian, B. Mechanisms and streams for processing of "what" and "where" in auditory cortex. *Proc Natl Acad Sci U S A* **97**, 11800-11806 (2000).
24. Russ, B.E., Orr, L.E. & Cohen, Y.E. Prefrontal neurons predict choices during an auditory same-different task. *Curr Biol* **18**, 1483-1488 (2008).
25. Bizley, J.K. & Cohen, Y.E. The what, where and how of auditory-object perception. *Nat Rev Neurosci* **14**, 693-707 (2013).
26. Ratcliff, R. & McKoon, G. The diffusion decision model: theory and data for two-choice decision tasks. *Neural Comput* **20**, 873-922 (2008).
27. Wichmann, F.A. & Hill, N.J. The psychometric function: I. Fitting, sampling, and goodness of fit. *Perception & Psychophysics* **63**, 1293-1313 (2001).
28. Cohen, M.R. & Newsome, W.T. Estimates of the Contribution of Single Neurons to Perception Depend on Timescale and Noise Correlation. *J Neurosci* **29**, 6635-6648 (2009).
29. Bizzi, E. Discharge of frontal eye field neurons during saccadic and following eye movements in unanesthetized monkeys. *Experimental Brain Research* **6**, 69-80 (1968).
30. Funahashi, S., Bruce, C.J. & Goldman-Rakic, P.S. Neuronal activity related to saccadic eye movements in the monkey's dorsolateral prefrontal cortex. *J Neurophysiol* **65**, 1464-1483 (1991).
31. Tsujimoto, S. & Sawaguchi, T. Neuronal representation of response-outcome in the primate prefrontal cortex. *Cereb Cortex* **14**, 47-55 (2004).
32. Sutton, R.S. & Barto, A.G. *Reinforcement learning : an introduction* (MIT Press, Cambridge, Mass., 1998).
33. Kiani, R. & Shadlen, M.N. Representation of confidence associated with a decision by neurons in the parietal cortex. *Science* **324**, 759-764 (2009).
34. Kepecs, A., Uchida, N., Zariwala, H.A. & Mainen, Z.F. Neural correlates, computation and behavioural impact of decision confidence. *Nature* **455**, 227-231 (2008).
35. Cohen, Y.E.*, et al.* A functional role for the ventrolateral prefrontal cortex in non-spatial auditory cognition. *Proc Natl Acad Sci U S A* **106**, 20045-20050 (2009).
36. Lee, J.H., Russ, B.E., Orr, L.E. & Cohen, Y.E. Prefrontal activity predicts monkeys' decisions during an auditory category task. *Fron Integrative Neuroscience* **3** (2009).
37. Bizley, J.K. & Cohen, Y.E. The what, where, and how of auditory-object perception. *Nat Rev Neurosci* **14**, 693-707 (2013).
38. Kim, J.N. & Shadlen, M.N. Neural correlates of a decision in the dorsolateral prefrontal cortex of the macaque. *Nat Neurosci* **2**, 176-185 (1999).
39. Fritz, J.B., David, S.V., Radkte-Schuller, S., Yin, P. & Shamma, S.A. Adaptive, behaviorally gated, persistent encoding of task-relevant auditory information in ferret frontal cortex. *Nat Neurosci* **13**, 1011-1019 (2010).
40. Tsujimoto, S. & Postle, B.R. The prefrontal cortex and oculomotor delayed response: a reconsideration of the "mnemonic scotoma". *J Cogn Neurosci* **24**, 627-635 (2012).
41. Zaksas, D. & Pasternak, T. Directional signals in the prefrontal cortex and in area MT during a working memory for visual motion task. *J Neurosci* **26**, 11726-11742 (2006).
42. Jun, J.K.*, et al.* Heterogenous population coding of a short-term memory and decision task. *J Neurosci* **30**, 916-929 (2010).
43. Lundqvist, M.*, et al.* Gamma and Beta Bursts Underlie Working Memory. *Neuron* **90**, 152-164 (2016).
44. Brody, C.D., Hernandez, A., Zainos, A. & Romo, R. Timing and neural encoding of somatosensory parametric working memory in macaque prefrontal cortex. *Cereb Cortex* **13**, 1196-1207 (2003).
45. Schmitt, L.I.*, et al.* Thalamic amplification of cortical connectivity sustains attentional control. *Nature* **545**, 219-+ (2017).

46. Murray, J.D., *et al.* Stable population coding for working memory coexists with heterogeneous neural dynamics in prefrontal cortex. *Proc Natl Acad Sci U S A* **114**, 394-399 (2017).
47. Pouget, A., Dayan, P. & Zemel, R. Information processing with population codes. *Nat Rev Neurosci* **1**, 125-132. (2000).
48. Kohn, A., Coen-Cagli, R., Kanitscheider, I. & Pouget, A. Correlations and Neuronal Population Information. *Annu Rev Neurosci* **39**, 237-256 (2016).
49. Averbeck, B.B., Latham, P.E. & Pouget, A. Neural correlations, population coding and computation. *Nat Rev Neurosci* **7**, 358-366 (2006).
50. Meyers, E.M. Dynamic population coding and its relationship to working memory. *J Neurophysiol* **120**, 2260-2268 (2018).
51. Meister, M.L., Hennig, J.A. & Huk, A.C. Signal multiplexing and single-neuron computations in lateral intraparietal area during decision-making. *J Neurosci* **33**, 2254-2267 (2013).
52. Tsunada, J., Baker, A.E., Christison-Lagay, K.L., Davis, S.J. & Cohen, Y.E. Modulation of cross-frequency coupling by novel and repeated stimuli in the primate ventrolateral prefrontal cortex. *Front Psychology* **2** (2011).
53. Frey, S., Comeau, R., Hynes, B., Mackey, S. & Petrides, M. Frameless stereotaxy in the nonhuman primate. *Neuroimage* **23**, 1226-1234 (2004).
54. Romanski, L.M. & Goldman-Rakic, P.S. An auditory domain in primate prefrontal cortex. *Nat Neurosci* **5**, 15-16 (2002).
55. Russ, B.E., Ackelson, A.L., Baker, A.E. & Cohen, Y.E. Coding of auditory-stimulus identity in the auditory non-spatial processing stream. *J Neurophysiol* **99**, 87-95 (2008).
56. Ding, L. & Gold, J.I. Separate, Causal Roles of the Caudate in Saccadic Choice and Execution in a Perceptual Decision Task. *Neuron*, 865-874 (2012).
57. Graziano, M.S., Aflalo, T. & Cooke, D.F. Arm movements evoked by electrical stimulation in the motor cortex of monkeys. *J Neurophysiol* **94**, 4209-4223 (2005).
58. Armstrong, K.M. & Moore, T. Rapid enhancement of visual cortical response discriminability by microstimulation of the frontal eye field. *Proc Natl Acad Sci U S A* **104**, 9499-9504 (2007).
59. Hanks, T.D., Ditterich, J. & Shadlen, M.N. Microstimulation of macaque area LIP affects decision-making in a motion discrimination task. *Nat Neurosci* **9**, 682-289 (2006).
60. Gold, J.I. & Shadlen, M.N. Banburismus and the brain: decoding the relationship beteween sensory stimuli, decisions, and reward. *Neuron* **36**, 299-308 (2002).
61. Eckhoff, P., Holmes, P., Law, C., Connolly, P.M. & Gold, J.I. On diffusion processes with variable drift rates as models for decision making during learning. *New J Phys* **10**, nihpa49499 (2008).
62. Ratcliff, R., Van Zandt, T. & McKoon, G. Connectionist and diffusion models of reaction time. *Psychol Rev* **106**, 261-300 (1999).
63. Green, C.S., Pouget, A. & Bavelier, D. Improved probabilistic inference as a general learning mechanism with action video games. *Curr Biol* **20**, 1573-1579 (2010).
64. Mulder, M.J., *et al.* The speed and accuracy of perceptual decisions in a random-tone pitch task. *Atten Percept Psychophys* **75**, 1048-1058 (2013).
65. Brunton, B.W., Botvinick, M.M. & Brody, C.D. Rats and humans can optimally accumulate evidence for decision-making. *Science* **340**, 95-98 (2013).
66. Shadlen, M.N., Hanks, T.D., Churchland, A., Kiani, R. & Yang, T. The Speed and Accuracy of a Simple Perceptual Decision: A Mathematical Primer. in *Bayesian Brain: Probabilistic Approaches to Neural Coding* (ed. K. Doya, S. Ishii, R. Rao & A. Pouget) (MIT Press, Cambridge, MA, 2006).
67. Salzman, C.D., Britten, K.H. & Newsome, W.T. Cortical microstimulation influences perceptual judgements of motion direction. *Nature* **346**, 174-177 (1990).

68. Cox, D.R. *Analysis of binary data* (Methuen, London, 1970).
69. Roitman, J.D. & Shadlen, M.N. Response of neurons in the lateral intraparietal area during a combined visual discrimination reaction time task. *J Neurosci* **22**, 9475-9489 (2002).
70. Selezneva, E., Scheich, H. & Brosch, M. Dual Time Scales for Categorical Decision Making in Auditory Cortex. *Curr Biol* **16**, 2428-2433 (2006).
71. Tsunada, J., Lee, J.H. & Cohen, Y.E. Representation of speech categories in the primate auditory cortex. *J Neurophysiol* **105**, 2634-2646 (2011).
72. Meyers, E.M., Freedman, D.J., Kreiman, G., Miller, E.K. & Poggio, T. Dynamic population coding of category information in inferior temporal and prefrontal cortex. *J Neurophysiol* **100**, 1407-1419 (2008).
73. Bishop, C.M. Pattern Recognition and Machine Learning. *Springer* (2006).

Figure Legends

Figure 1: **Task and stereotactic location of vlPFC**. **a,** Each monkey decided whether a temporal sequence of tone bursts was predominantly “low frequency” or “high frequency” and responded with a rightward or leftward movement, respectively, of the joystick. The monkey could report its choice any time after stimulus onset. **b,** vlPFC (pink square) is ventral to the posterior aspect of the principal sulcus (PC) and anterior to the arcuate sulcus (AS)[54]. The dotted box indicates the circumference of the recording chamber. Arrows indicate the anterior (A)-posterior (P) axis and the medial (M)-lateral (L) axis.

Figure 2: **Psychophysical performance on the low-high task**. Psychometric (**a**) and chronometric (**b**) functions for Monkey T (top) and Monkey A (bottom). These functions were generated from their responses on the current trial. Psychometric functions are plotted as the percentage of trials in which a monkey chose “high frequency” as a function of signed coherence, in which larger negative/positive coherence values indicate more low/high frequency tone bursts. The horizontal grey lines on the psychometric plots indicate lapse rates (errors for strong stimuli, presumably reflecting lapses in attention or inappropriate application of the decision-motor mapping), which were estimated from logistic fits (solid blue lines). Chronometric functions are plotted using the mean RT, which was the time interval between stimulus onset and onset of joystick movement. Grey dots are low-frequency choices, and black dots are high-frequency choices. Solid pink curves are simultaneous fits of both the psychometric and chronometric data to a drift-diffusion model (DDM). The horizontal dashed grey lines on the chronometric plots indicate choice-dependent non-decision times (NDT) estimated by the DDM fits. Decision times (DT) were estimated as the difference between the trial-specific RT and the choice-specific NDT. **c,** Psychometric functions computed separately for different sequential conditions, as indicated in the top panel. **d,** Distributions of best-fitting, session-by-session coefficients from the logistic fits: β_0, overall choice bias; β_1, sensitivity to coherence; β_2, the

tendency to repeat a correct choice; and β_3, the tendency to repeat an erroneous choice. Filled data points indicate likelihood-ratio test, H_0: regression coefficient equals 0, $p<0.05$. Horizontal bars indicate median values; red bars indicate Wilcoxon sign-rank test, H_0: median value equals 0, $p<0.05$.

Figure 3: **Neuronal sensitivity to choice in single vlPFC neurons**. (**a**-**d**) The left plots are raster and peristimulus-time histograms from correct trials only showing sensitivity to low-frequency (<0% coherence; red) and high-frequency choices (>0% coherence; blue). The thick lines indicate mean firing rate, and the dotted lines indicate the 95% confidence intervals. Data are aligned relative to stimulus onset. Grey circles in the raster plots indicate the time of onset of joystick movement. The middle plots show the responses of the same neurons but aligned relative to the onset of joystick movement. The arrow indicates the time of peak choice selectivity. The right plot summarizes each neuron's firing rate during its peak firing rate ±100 ms: correct low-frequency choices are shown in red, high-frequency choices in blue, and incorrect choices in grey (only for coherences with at least 5 trials). Error bars indicate the standard error of the mean.

Figure 4: **Population selectivity for vlPFC neurons**. **a,** Summary of choice selectivity. Data from individual neurons are sorted by the onset of choice selectivity (open circles), defined as the first of three consecutive time bins for which Wilcoxon rank-sum test, H_0: no median difference in firing rates for the two choices, $p<0.05$, FDR corrected. Color indicates the ROC value of choice selectivity from correct trials (see legend). Rows show data for high (<-80% versus >+80%), middle (-80% to -20% versus +80% to +20%), and low (-20% to 0 versus 0 to +20%) coherence trials, as indicated. **b,** Percentage of neurons with significant selectivity for choice or coherence (Wilcoxon rank-sum test for H_0: no median difference in firing rates elicited by high- versus middle- coherence stimuli for each choice, $p<0.05$, FDR corrected) computed in

300-ms time bins with 10-ms steps. Choice selectivity is shown separately for high, middle, and low coherences, as indicated. Red points indicate times corresponding to a significant difference in the proportion of choice-selective neurons at each coherence level (running χ^2-test for H_0: proportion is the same, $p<0.05$, FDR corrected). Coherence selectivity is shown in dark red for preferred choices (i.e., the choice direction that elicits higher firing rates) and light red for non-preferred choices. In the leftmost panel, the horizontal bars represent the range of the inferred times of the decision commitment for high (black), middle (dark grey), and low (light grey) coherence stimuli (the range is indicated by the large vertical bar). In **a** and **b**, the data in each panel are aligned relative to different task epochs (from left to right): stimulus onset, inferred decision commitment, onset of joystick movement, and time of reward delivery.

Figure 5: **Choice selectivity on correct and error trials.** Scatterplots showing, on a neuron-by-neuron basis, the peak ROC choice-selectivity value computed on correct versus error trials. Both values were computed from spiking data occurring at the time of peak ROC-based choice selectivity from correct trials for the given neuron. Black/gray points correspond to data from high/middle coherence stimuli. The line in each panel is the line of unity. The panels show data computed relative to different task epochs (from left to right): stimulus onset, inferred decision commitment, onset of joystick movement, and time of reward delivery. Across all epochs, error ROC values tended to be smaller than peak ROC values (Wilcoxon sign-rank test for H_0: median ROC values are the same, $p<0.05$). Different panels have different numbers of data points because for some sessions, there were not enough trials to reliably calculate the error ROC.

Figure 6: **Classifier analysis.** The ability of a linear classifier to determine from the population of vlPFC neurons the current choice (low frequency [-100%–0%] vs. high frequency choice

[0%–100%]; **a**) and stimulus coherence (<-50% versus -50%–0% versus 0%–+50% versus >+50%; **b**), computed using correct trials only in 300-ms time bins with 10-ms steps. Thick lines represent median decoding performance; dashed lines are the interquartile range. In the leftmost panel, the horizontal bar represent the range of the inferred times of the decision commitment for high (black), middle (dark grey), and low (light grey) coherence (the range is indicated by the large vertical bars). Choice- and coherence-decoding performance is aligned relative to different task epochs (from left to right): stimulus onset, inferred decision commitment, onset of joystick movement, and time of reward delivery. We did not conduct a classifier analysis on error trials because there was not enough data to generate reliable results.

Figure 7: **Choice selectivity for the current and next trial**. For Monkey T (top) and Monkey A (bottom), choice selectivity is plotted as a function of time relative to the onset of joystick movement (**a**) and reward delivery (**b**). Lines indicate ROC-based choice selectivity computed in 300-ms time bins, with 10-ms steps from pooled spiking data across all recorded neurons (z-scored per neuron) that contributed at least 121 for monkey T and 54 trials for monkey A under the given conditions. Solid/dotted lines correspond to correct/error outcomes on the current trial. Black lines indicate selectivity for repeated (ROC values >0.5) versus switched (<0.5) choices on the next trial, relative to the choice on the current trial (i.e., values >0.5 imply that the neuronal population tended to respond more in anticipation of a repeated choice). For reference, gray lines indicate selectivity for the preferred choices on the current trial (i.e., values >0.5 indicate, by definition, selectivity for the choice that elicited the larger average spike rate during peak firing rate ±100 ms for each neuron). Red points, computed only for the black curves, indicate permutation test for H_o: ROC value equals 0.5, $p<0.05$.

Figure 8: **Effect of microstimulation on behavioral performance on the current and next trial**. **a** and **b,** Single-site examples of the effects of vlPFC microstimulation on psychometric performance on the current trial for a low-choice site (**a**) and a high-choice site (**b**). Psychometric functions are plotted as in Fig. 2. Red/blue symbols are for data from trials with/without microstimulation. Solid lines are logistic fits, computed separately for the two conditions. Dotted lines are 95% confidence intervals of the non-microstimulation trials that were calculated by a bootstrap procedure[56]. **c** and **d**, Scatterplots showing session-by-session effects of microstimulation on the correlation between neuronal choice selectivity and the percent change in psychometric choice bias (**c**; Spearman's rank correlation coefficient ρ=0.15, p=0.42) and the change in psychometric threshold (**d**; ρ=0.15, p=0.43) of the current decision. **e and f,** Single-site examples of microstimulation's effects on psychometric performance on the next trial for a low-choice site (**e**) and a high-choice site (**f**). The data are formatted in the same manner as panels **a** and **b**. **g** and **h**, Scatterplots show session-by-session effects of microstimulation on the correlation between neuronal choice selectivity and the percent change in psychometric choice bias (**g**; ρ=0.6, p=0.0003) and the change in psychometric threshold (**h**; ρ=0.11, p=0.56) of the next decision. Filled data points are significant single-session microstimulation-induced changes in the given psychometric property (permutation test, p<0.05).

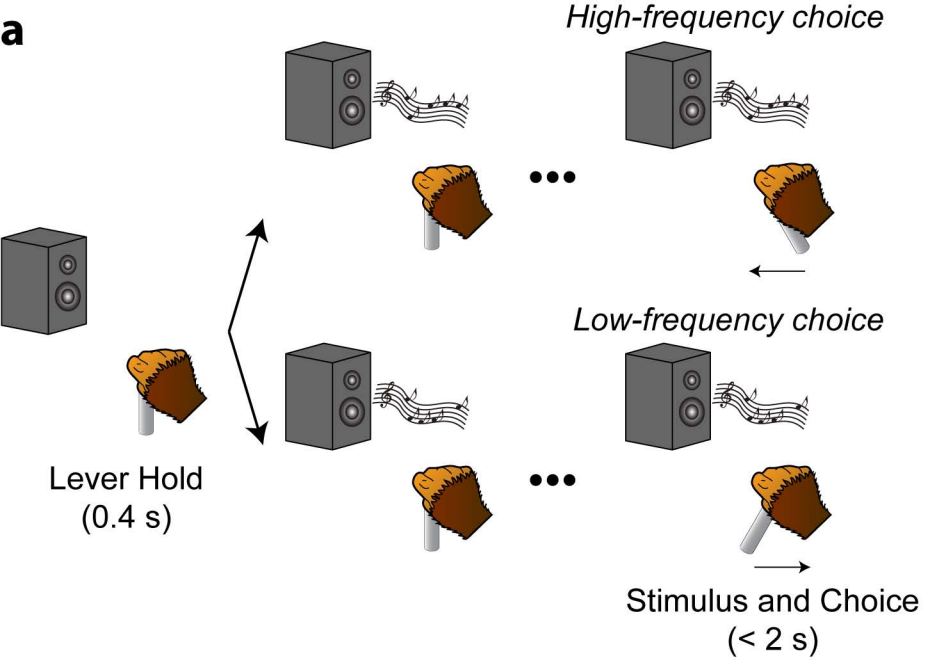
a
High-frequency choice
Low-frequency choice
Lever Hold
(0.4 s)
Stimulus and Choice
(< 2 s)

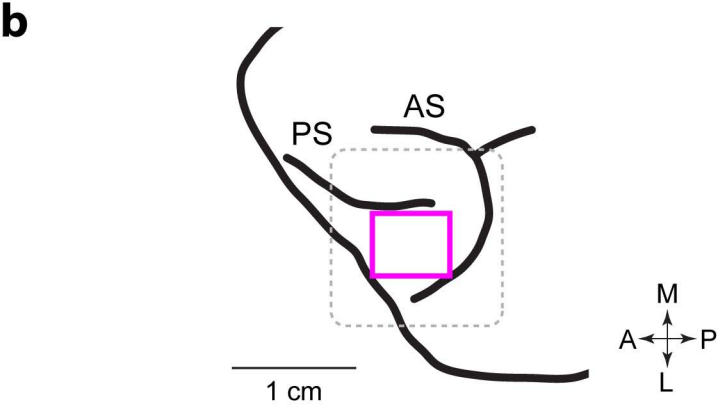
b
PS
AS
1 cm
M
A
P
L

Figure 1.

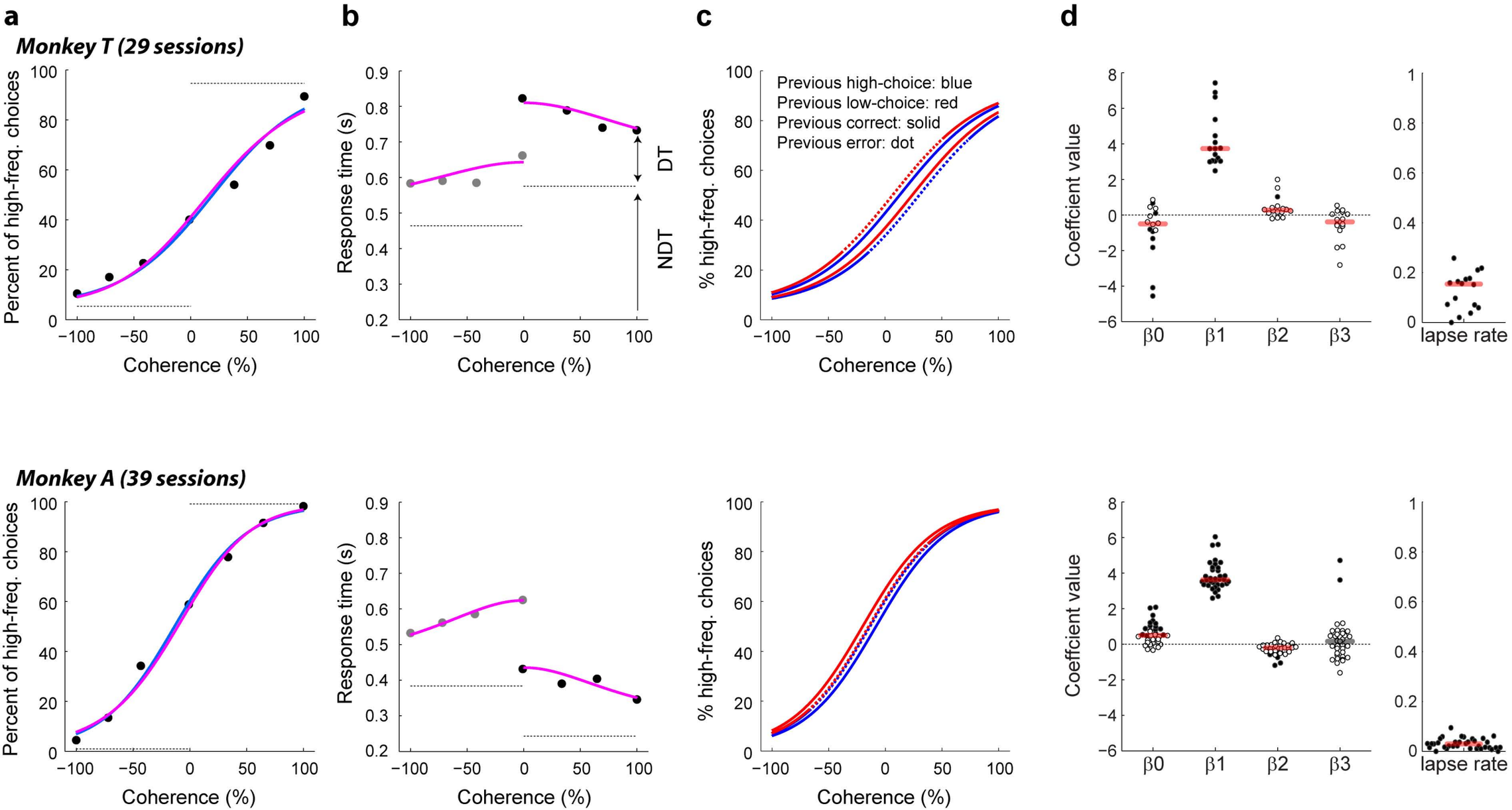
a
Monkey T (29 sessions)
Percent of high-freq. choices
Coherence (%)
b
Response time (s)
DT
NDT
Coherence (%)
c
Previous high-choice: blue
Previous low-choice: red
Previous correct: solid
Previous error: dot
% high-freq. choices
Coherence (%)
d
Coeffcient value
β0
β1
β2
β3
lapse rate
Monkey A (39 sessions)
Percent of high-freq. choices
Coherence (%)
Response time (s)
Coherence (%)
% high-freq. choices
Coherence (%)
Coeffcient value
β0
β1
β2
β3
lapse rate

Figure 2.

Figure 3.

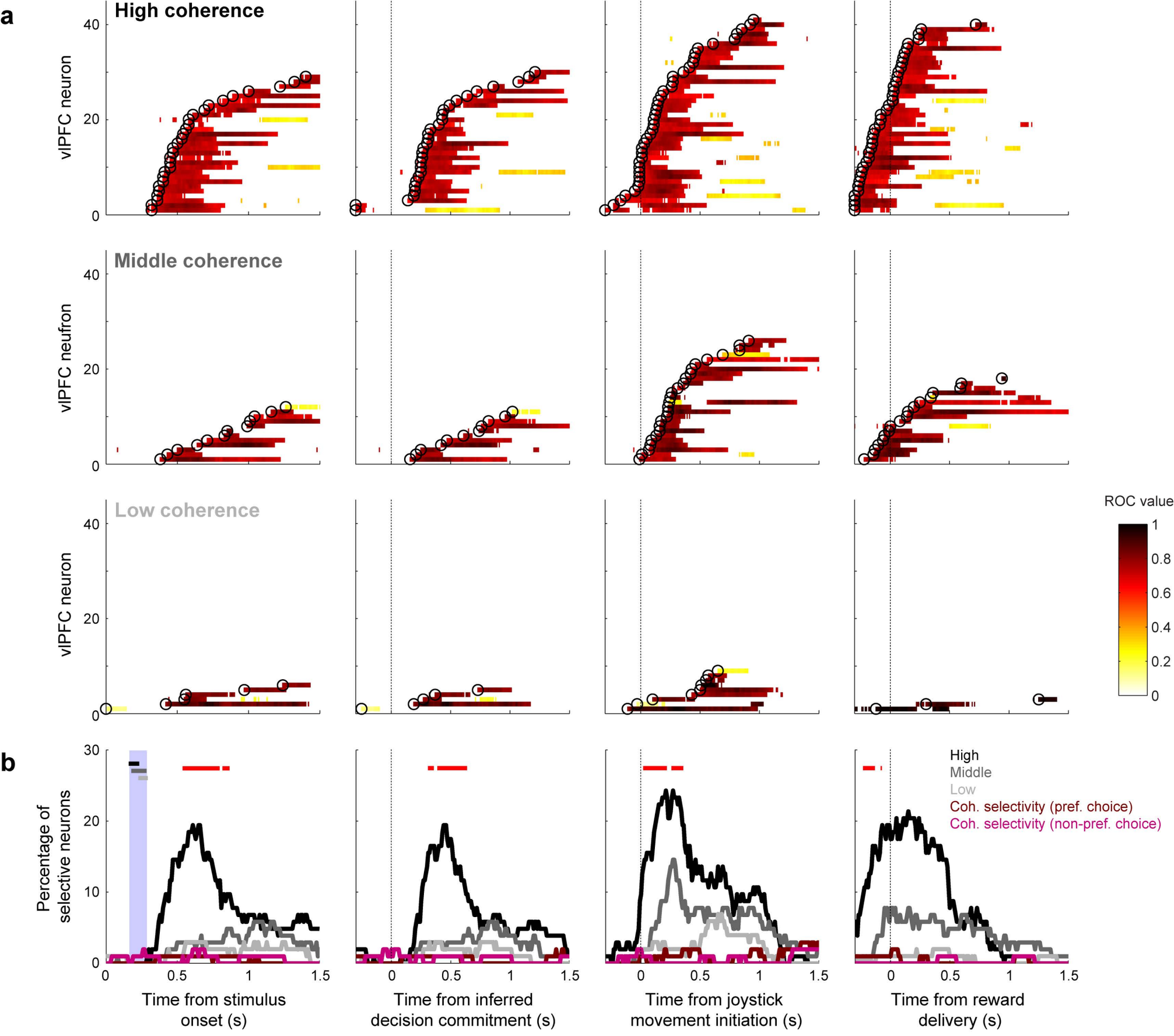
a
High coherence
Middle coherence
Low coherence
vlPFC neuron
vlPFC neufron
40
20
0
ROC value
1
0.8
0.6
0.4
0.2
0
b
Percentage of selective neurons
30
20
10
0
0.5
1
1.5
High
Middle
Low
Coh. selectivity (pref. choice)
Coh. selectivity (non-pref. choice)
Time from stimulus onset (s)
Time from inferred decision commitment (s)
Time from joystick movement initiation (s)
Time from reward delivery (s)

Figure 4.

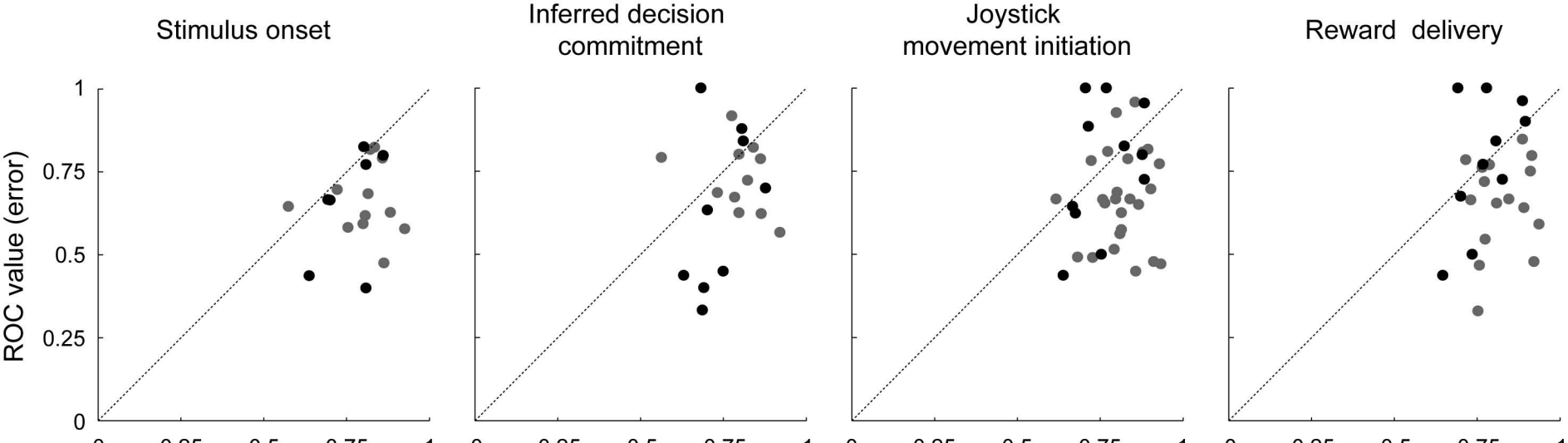
Stimulus onset
Inferred decision commitment
Joystick movement initiation
Reward delivery
ROC value (error)
ROC value (correct)
0
0.25
0.5
0.75
1

Figure 5.

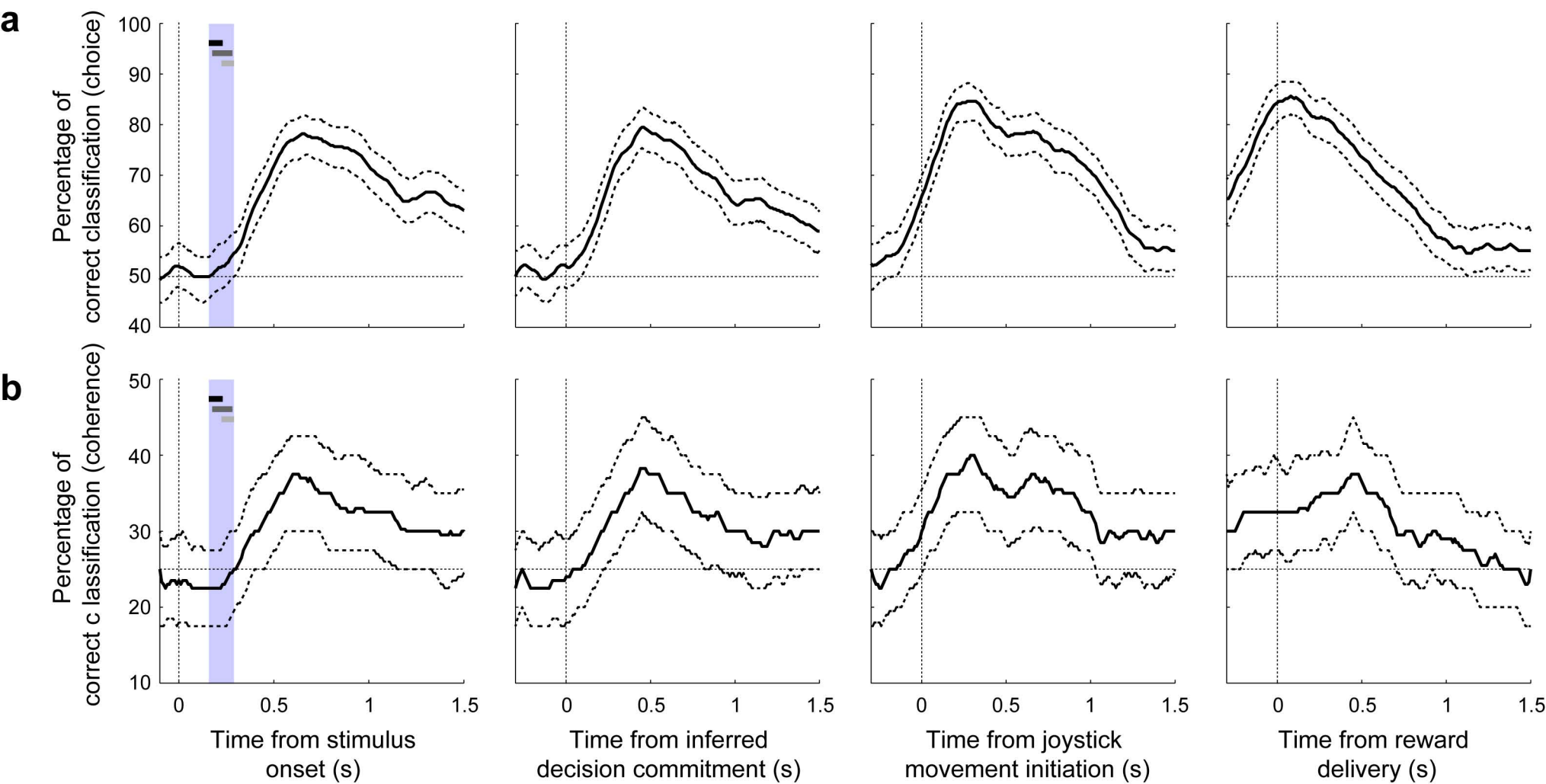
a
b
Percentage of correct classification (choice)
Percentage of correct c lassification (coherence)
100
90
80
70
60
50
40
30
20
10
0
0.5
1
1.5
Time from stimulus onset (s)
Time from inferred decision commitment (s)
Time from joystick movement initiation (s)
Time from reward delivery (s)

Figure 6.

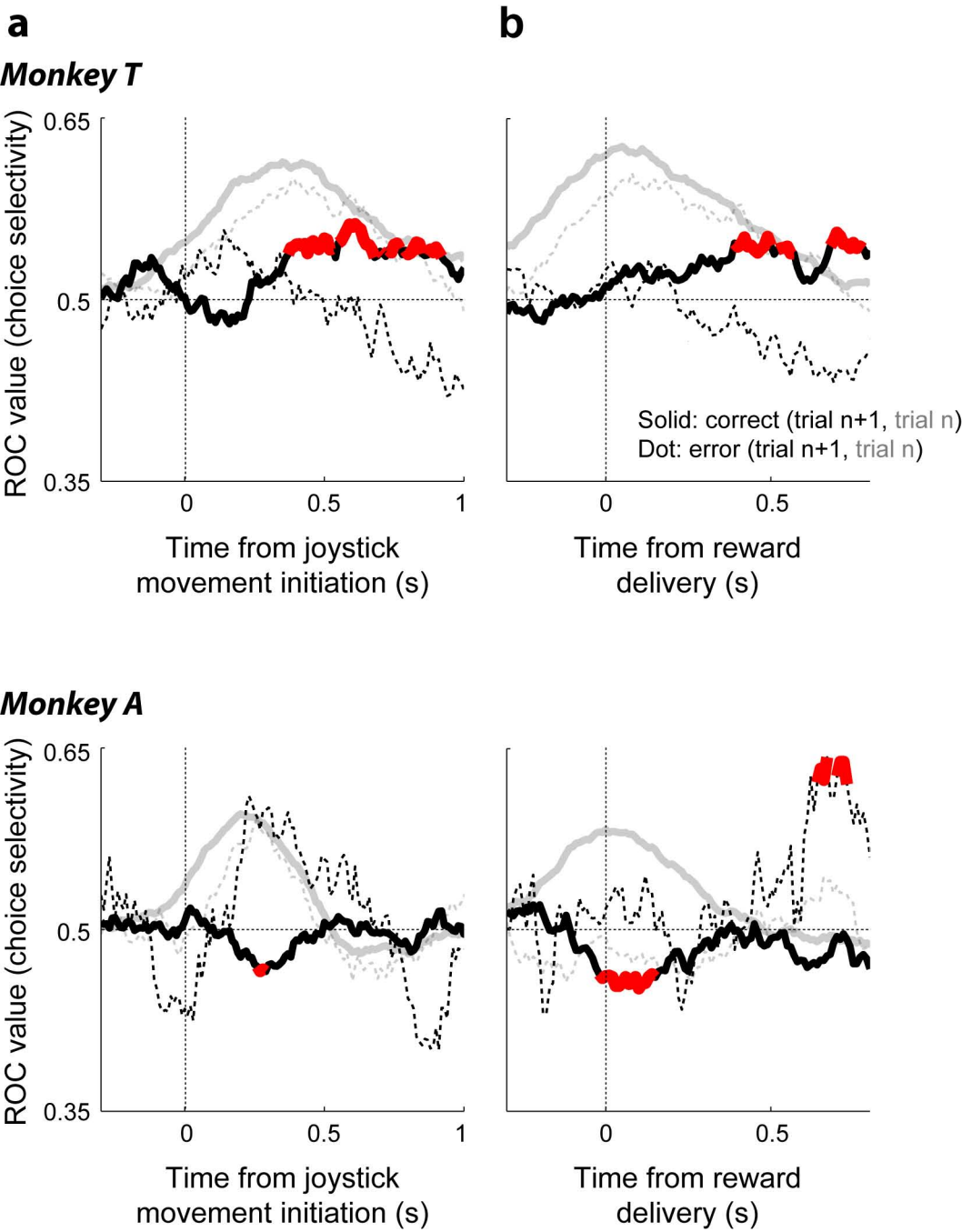
a
b
Monkey T
ROC value (choice selectivity)
0.65
0.5
0.35
0
0.5
1
Time from joystick movement initiation (s)
Time from reward delivery (s)
Solid: correct (trial n+1, trial n)
Dot: error (trial n+1, trial n)
Monkey A

Figure 7.

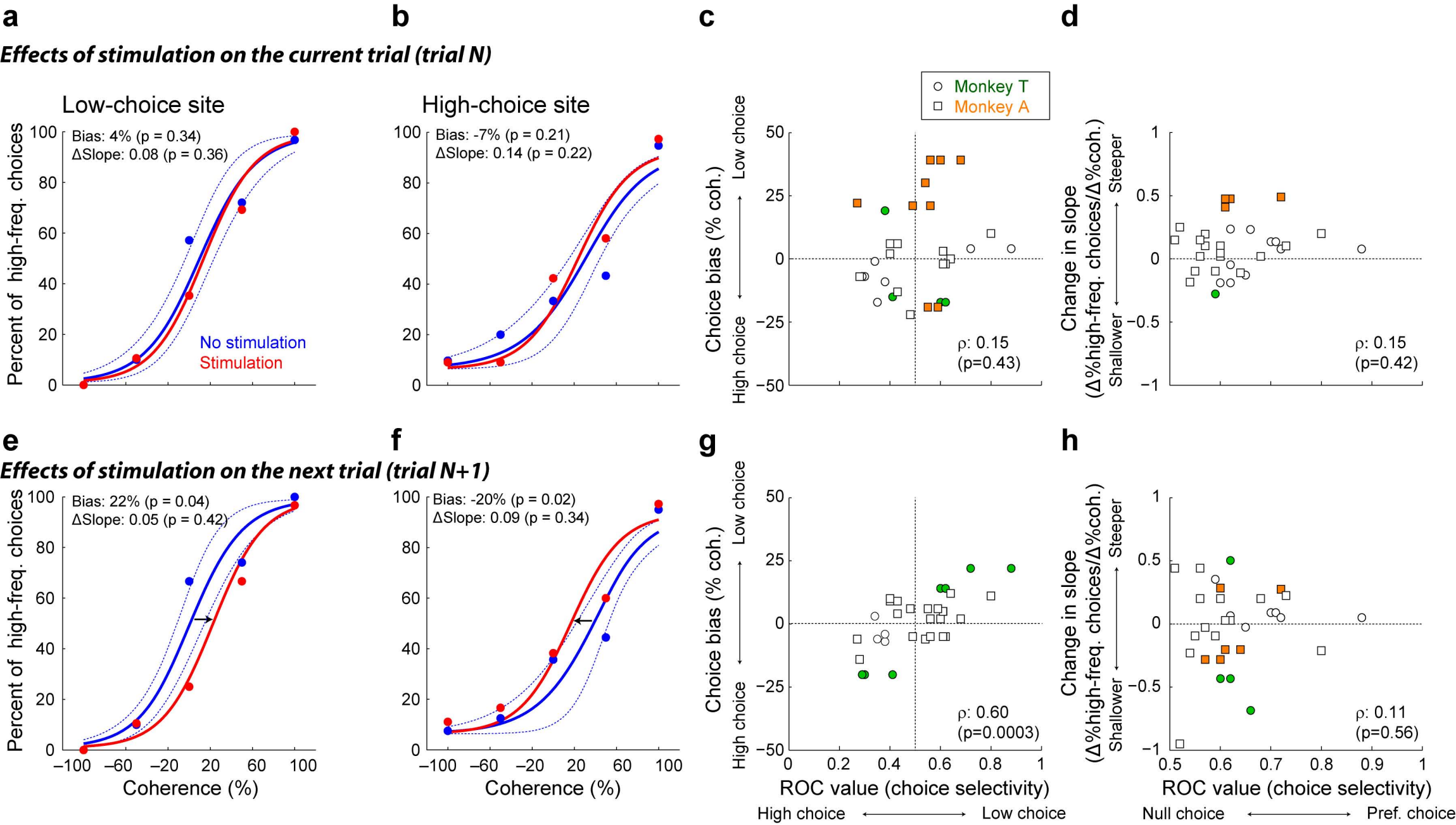
a
b
c
d
Effects of stimulation on the current trial (trial N)
Low-choice site
High-choice site
Bias: 4% (p = 0.34)
ΔSlope: 0.08 (p = 0.36)
Bias: -7% (p = 0.21)
ΔSlope: 0.14 (p = 0.22)
Percent of high-freq. choices
No stimulation
Stimulation
Monkey T
Monkey A
Choice bias (% coh.)
Low choice
High choice
ρ: 0.15
(p=0.43)
Change in slope
(Δ%high-freq. choices/Δ%coh.)
Steeper
Shallower
ρ: 0.15
(p=0.42)
e
f
g
h
Effects of stimulation on the next trial (trial N+1)
Bias: 22% (p = 0.04)
ΔSlope: 0.05 (p = 0.42)
Bias: -20% (p = 0.02)
ΔSlope: 0.09 (p = 0.34)
Coherence (%)
ρ: 0.60
(p=0.0003)
ROC value (choice selectivity)
High choice
Low choice
ρ: 0.11
(p=0.56)
Null choice
Pref. choice

Figure 8.